Superconducting phase qubits with shadow-evaporated Josephson junctions*

Fei-Fan Su(宿非凡)[1,2], Wei-Yang Liu(刘伟洋)[1,2], Hui-Kai Xu(徐晖凯)[1,2], Hui Deng(邓辉)[1], Zhi-Yuan Li(李志远)[1,3], Ye Tian(田野)[1], Xiao-Bo Zhu(朱晓波)[4], Dong-Ning Zheng(郑东宁)[1], Li Lv(吕力)[1], and Shi-Ping Zhao(赵士平)[1,2,5,†]

[1] *Beijing National Laboratory for Condensed Matter Physics, Institute of Physics, Chinese Academy of Sciences, Beijing* 100190, *China*
[2] *School of Physical Sciences, University of Chinese Academy of Sciences (CAS), Beijing* 100049, *China*
[3] *National Laboratory of Solid State Microstructures, School of Physics, Nanjing University, Nanjing* 210093, *China*
[4] *CAS Center for Excellence and Synergetic Innovation Center in Quantum Information and Quantum Physics, University of Science and Technology of China, Hefei* 230026, *China*
[5] *Collaborative Innovation Center of Quantum Matter, Beijing, China*

(Received 13 January 2017; revised manuscript received 28 February 2017; published online 10 May 2017)

We develop a fabrication process for the superconducting phase qubits in which Josephson junctions for both the qubit and superconducting quantum interference device (SQUID) detector are prepared by shadow evaporation with a suspended bridge. Al junctions with areas as small as 0.05 μm^2 are fabricated for the qubit, in which the number of the decoherence-causing two-level systems (TLS) residing in the tunnel barrier and proportional to the junction area are greatly reduced. The measured energy spectrum shows no avoided crossing arising from coherent TLS in the experimentally reachable flux bias range of the phase qubit, which demonstrates the energy relaxation time T_1 and dephasing time T_φ on the order of 100 ns and 50 ns, respectively. We discuss several possible origins of decoherence from incoherent or weakly-coupled coherent TLS and further improvements of the qubit performance.

Keywords: superconducting phase qubit, two-level system, decoherence, shadow evaporated junction

PACS: 03.67.Lx, 03.65.Yz, 85.25.Cp, 74.50.+r **DOI:** 10.1088/1674-1056/26/6/060308

1. Introduction

Superconducting quantum bits (qubits)[1] play a central role in superconducting quantum circuits, which are a promising candidate for solid-state quantum computing[2] and can serve as an excellent platform for the studies of quantum optics[3] and quantum simulation.[4] In addition to the various types of qubits such as charge, flux, and transmon (or Xmon),[1] the superconducting phase qubits[5–17] have been received much attention in the past years due to their unique properties and advantages. It is known that the phase qubit has a widely tunable anharmonicity α ranging from 0.1% to 10%, and it is convenient to couple the qubits capacitively or inductively, leading to the rich Hamiltonians that are desirable for developing circuit architectures for quantum simulators. The phase qubit is also unique in exploring some physical phenomena such as macroscopic quantum tunneling.[12]

The fabrication of superconducting phase qubits usually employs multilayer techniques with wiring crossovers.[8] For the fabrication of the qubit junction, an Al underlayer (or the junction's base electrode) is first sputter deposited and then patterned. It is cleaned via Ar–ion milling before thermal oxidation for the formation of the tunnel barrier. Afterwards, another Al layer is deposited and patterned to complete the junction counter electrode. In order to avoid the junction's tunnel barrier formed on the Ar–ion milled surface of Al that may lead to possible barrier defects, the *in-situ* trilayer junction formation[9] and the shadow evaporation technique without a suspended bridge[10] have been studied. In all these processes, the qubit junctions usually have micron-meter sizes, which show clear microscopic two-level systems (TLS) in the qubit spectrum, which reside in the tunnel barriers and are known to cause significant decoherence.[5,16,17]

The technique of shadow evaporation with a suspended bridge is now widely used for the fabrication of the charge-,[18,19] flux-,[20,21] and transmon- (or Xmon-)[22,23] type qubits, in which qubit junctions with sizes well below one micron can be conveniently produced so that the number of TLS in the tunnel barrier can be reduced. In this work we develop a fabrication process for the phase qubits in which Josephson junctions for both the qubit and SQUID detector are prepared by the technique of shadow evaporation with suspended bridge. Thermally oxidized Si substrates are used in this study, and Nb and Al films are used as the outer wiring and central qubit/SQUID detector parts of the device, respectively. Al junctions with areas as small as 0.05 μm^2 are fab-

*Project supported by the National Basic Research Program of China (Grant Nos. 2014CB921202, 2015CB921104, and 2016YFA0300601) and the National Natural Science Foundation of China (Grant Nos. 91321208 and 11674380).

†Corresponding author. E-mail: spzhao@iphy.ac.cn

© 2017 Chinese Physical Society and IOP Publishing Ltd

ricated for the qubit. We show that in contrast to the previous reports, no coherent TLS is present in the entire flux bias range of the phase qubit, which is confirmed by the numerical simulation of the qubit system. The measured results show the energy relaxation time T_1 and dephasing time T_φ on the order of 100 ns and 50 ns, respectively. We will discuss possible causes for the decoherence arising from incoherent TLS and further improvements of the phase qubit performance.

2. Qubit design and fabrication

The structure of the phase qubit can be seen schematically in Fig. 1, which consists of four parts: The qubit loop, the dc-SQUID detector, and the flux and microwave bias circuits. For the fabrication of the device, we followed the circuit design developed by the UCSB group,[7,8] including the qubit and SQUID loops, the shunt capacitances, and the bias circuits. The fabrication process, however, is substantially different such that the shadow evaporated Josephson junctions are incorporated into the device to replace the multilayer fabricated junctions.

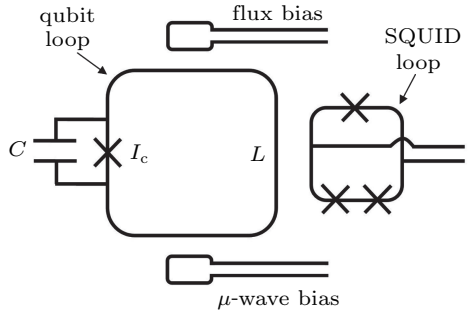


Fig. 1 Schematic rf-SQUID phase qubit with Josephson critical current I_c, shunt capacitance C, and loop inductance L. A 3-junction dc-SQUID is used to detect the qubit states.

Figure 2(a) shows the optical microscope image of the fabricated phase qubit. It can be seen that both flux and microwave bias circuits have two parts which are symmetrical to the dc-SQUID but not to the qubit loop so that field bias of the qubit will not change the detector state.[7,8] The inductance L of the qubit loop is designed to be 800 pH. The mutual inductance between qubit and SQUID and that between qubit and flux (microwave) bias circuits are designed to be 78 pH and 4 (2) pH, respectively. The mutual inductance between SQUID and flux or microwave bias circuits is negligible due to symmetry. The capacitor area for both the qubit and SQUID is 50 μm×50 μm and the thickness of the Si interlayer deposited by plasma enhanced CVD (PECVD) is 200 nm. The capacitance is estimated to be about 750 fF. The shadow evaporated junction area of the qubit is designed to be 0.12 μm×0.42 μm∼0.05 μm^2 and the critical current density is $J_c = 2000$ A/cm^2, corresponding to the critical current of I_c = 1 μA and $\beta_L = 2\pi LI_c/\Phi_0 = 2.43 > 1$, which ensures the qubit potential with two minima when it is biased appropriately. The SQUID detector contains three junctions, where a small junction is in parallel with two larger ones connected in series whose critical current is 1.7 times that of the small one. The advantage of the 3-junction SQUID is that it requires no external flux bias for the operation as a magnetometer. Figures 2(b) and 2(c) are the SEM images of the qubit junction and two junctions in one of the SQUID arms, formed by the shadow evaporated technique.

The fabrication of the phase qubit consists of the following five main steps, as illustrated in Fig. 2(d):

Step 1 First of all, a 150-nm thick Nb film is dc-sputter deposited on the 430-μm thick Si substrate. The substrate has resistivity above 5-kΩcm and a 500-nm thick SiO_2 surface layer. Sputtering is performed in an ultrahigh vacuum system whose background pressure is 2×10^{-6} Pa. The Ar working pressure is 1.5 Pa, and the sputtering voltage and current are 260 V and 0.4 A, respectively, which give rise to a deposition rate of 2.73 nm/s. The substrate holder is water cooled so that the sample temperature is kept below 100 °C during sputtering. The film is photolithographically patterned using S-1813 resist and dry etched via reactive ion etching in SF_6. After removing the resist in acetone, the base Nb layer, seen in Fig. 2(d) in gray, is completed.

Step 2 Preparation of the MAA/PMMA double layer for the first Al layer patterning and lift-off. A 195-nm thick MAA layer is first spin coated on the substrate and baked up at 170 °C for 2 min. A 305-nm thick PMMA A5 layer is coated afterward and baked up at 170 °C for 30 min. The double layer is e-beam exposed in a 20-keV Raith 150 system with step size of 20 nm, aperture diameter of 20 μm, and area dose of 260 μC/cm^2. It is developed at 24 °C for 75 s and fixed for 30 s. A 90-nm thick Al film is subsequently evaporated in a Plassys system and then lifted off, which completes the first Al layer, shown in Fig. 2(d) in green. The Plassys system has a background pressure of 2×10^{-8} Pa and a deposition rate of 0.99 nm/s is used.

Step 3 A 200-nm thick Si insulating layer is prepared in a plasma-enhanced chemical vapor deposition (PECVD) system with a background vacuum of 2×10^{-6} Pa. The film is prepared at 120 °C with the SiH_4 and Ar flow rates of 25 and 477 sccm, respectively, which give rise to a deposition rate of 0.57 nm/s. The Si film is then patterned with e-beam lithography using N-7520 and dry etching in SF_6. This completes the insulating layer shown in Fig. 2(d) as the half transparent layer. We note that the insulating layers for the qubit and SQUID capacitances and those for the wire crossovers in the bias circuits, which can be seen in Fig. 2(a) but not included in panel (d), are also prepared in this step.

Step 4 The second Al layer shown in Fig. 2(d) in blue is fabricated in the similar way as in Step 2. Since contacts

with the first Al layer (in green) need to be formed, an Ar ion milling cleaning is performed before the deposition of the second Al layer. We note that the counter electrodes of the capacitances and the wire crossings for the bias circuits are also prepared in this step, as can be seen in Fig. 2(a). (For some samples the wire crossings for the bias circuits are made in a separate process if strong ion milling is required.)

Step 5 Shadow evaporated Josephson junctions (the light gray parts with red crosses in Fig. 2(d)) for the qubit and SQUID detector are prepared in the Plassys system in this final step to complete the phase qubit device. Similar conditions to those in Step 2 are used for the MAA/PMMA double layer preparation for the lift-off process and a pre-cleaning in O_2/Ar mixing gases is performed. The thicknesses of the bottom and top Al layers of the junctions are 40 nm and 60 nm, respectively. An oxidation time of 30 minutes with oxygen flow rate of 197 sccm is used for the barrier formation, which leads to a J_c of 2000 A/cm^2.

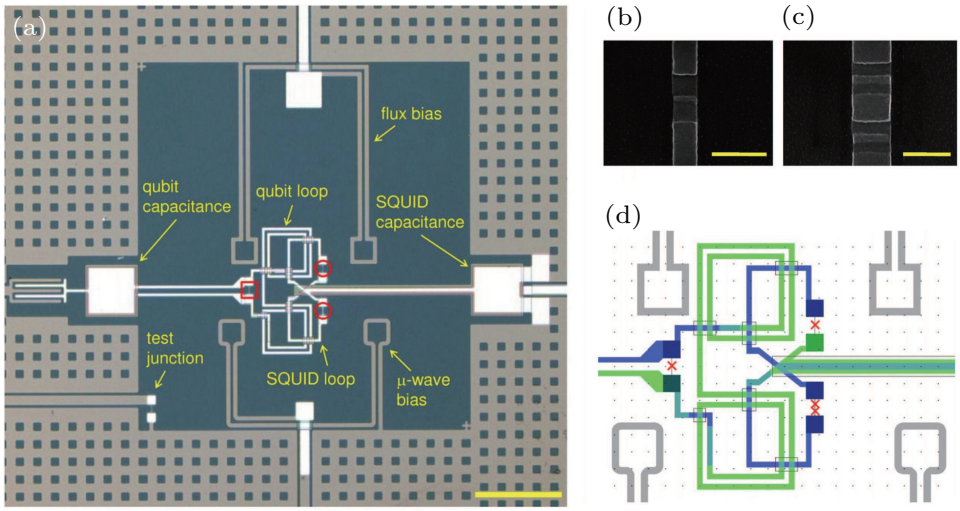


Fig. 2. (color online) (a) Optical microscope image of the central region of the fabricated phase qubit. The substrate appears greenish in color while the darker and brighter parts are the Nb and Al films. The interdigitated capacitor at the left side is used as a coupling to the neighboring component. The red open square and circles enclose the shadow evaporated junctions of the qubit and detector SQUID, respectively. SEM images of the qubit junction and two junctions in one of the SQUID arms are shown in panels (b) and (c). The design layout is illustrated in panel (d), in which the Nb (gray), the first Al (green), the Si (half transparent), the second Al (blue), and the shadow evaporated Al (light gray) films are prepared successively (see text for details). The horizontal bars at right-bottom corner in panels (a), (b), and (c) indicate lengths of 100, 1, and 1 μm, respectively. The grid cell dimension in panel (d) is 10 μm.

3. Results and discussion

Our primary goal is to reduce the influence from the TLS in the tunnel barrier on the qubit performance when small deep submicron sized, shadow evaporated qubit junctions are used. It is well known that when TLS is coherently coupled to the qubit system, its energy spectrum will exhibit clear avoided crossing at an energy corresponding to that of the TLS and with the split size representing the qubit-TLS coupling strength. In Fig. 3, we show the experimental energy spectrum of the fabricated phase qubit measured in a dry dilution refrigerator based system.[24] The measurement is performed by sending a continuous microwave, namely with its pulse width much larger than the qubit coherent time, and measuring the excited-state population right after the microwave signal ends. The flux bias and microwave frequency are swept with steps of $0.0025\Phi_0$ and 2 MHz, respectively. It can be seen that no avoided crossing is present in the experimentally measured flux bias range from $\Phi_e = 0.510\Phi_0$ to $\Phi_e = 0.565\Phi_0$, indicating that no TLS coherently coupled to the qubit with coupling strength above ~ 2 MHz is present.

Figure 4(a) shows the result from the qubit-TLS swap measurement in which the qubit excited-state population is recorded as time evolves for the frequency range corresponding to that of Fig. 3. In Fig. 4(b), we show the time sequence of the flux bias pulses (blue) and microwave π-pulse (green) for the measurement. The blue baseline indicates the flux bias level of $\Phi_e = 0.525\Phi_0$ (corresponding to the qubit level spacing of 7.55 GHz) at which a π-pulse is calibrated from Rabi oscillation measurement. The qubit is always excited first at this bias level and the flux bias is swept in the whole range by changing $\Delta\Phi_e$ (plus or minus), which continues for a time t before the readout pulse is applied. Consistent with the result of the energy spectrum in Fig. 3, no interference pattern arising from the exchange of energy between the qubit and TLS is seen. This further demonstrates that there is no TLS in the tunnel barrier coherently coupled to the qubit, with a lower bound of the coupling strength set by the qubit coherent times. From the result the time dependence of excited-state population still shows clear differences when the frequency changes. The influence of the incoherent or weakly-coupled coherent TLS may be the cause for these differences, which could reduce the coherent times of the qubit. In fact, the measured

relaxation time T_1 (see the inset of Fig. 3) and dephasing time T_φ from Ramsey fringe measurement (not shown) at the qubit level spacing of 7.55 GHz are around 100 ns and 50 ns, respectively, which are a few factors lower than the best phase qubits reported previously.[8]

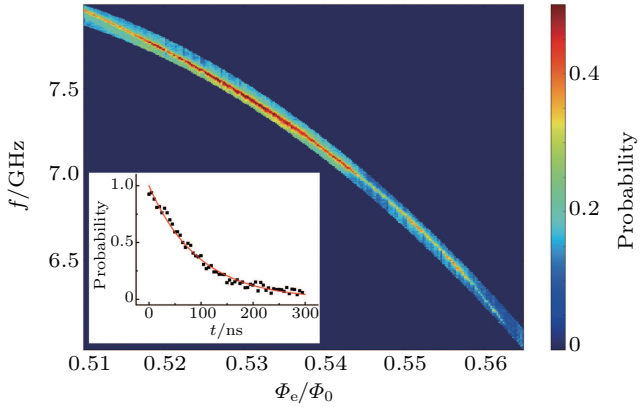


Fig. 3. (color online) Energy spectroscopy of the fabricated phase qubit measured at 20 mK. Note that for the whole measurable qubit level spacing ranging from about 6 GHz to 8 GHz, no avoided crossing from coherent barrier TLS is seen. Inset shows the measured energy relaxation with $T_1 = 95.4$ ns at the qubit level spacing of 7.55 GHz.

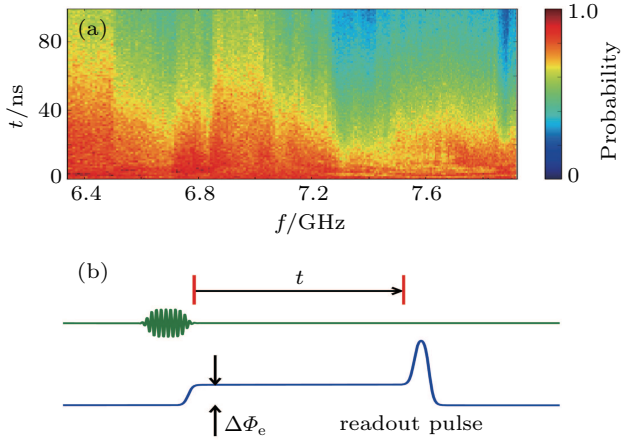


Fig. 4. (color online) (a) Swap spectroscopy of the phase qubit showing no oscillation patterns from coherently coupled barrier TLS. (b) The timing of the flux bias pulses (blue) and microwave π-pulse (green) for the measurement.

In order to see how the qubit potential wells and energy levels vary with the applied flux bias, we use two approaches to determine the qubit parameters I_c (or β_L), L, and C. The first approach is to determine the β_L and LC parameters from the energy spectrum, and the parameter L/C from the macroscopic resonant tunneling measurement.[25] The second approach is to calculate the qubit level spacing versus applied flux bias via the Fourier grid Hamiltonian method[26] with I_c, L, and C as adjustable parameters. The two approaches produce approximately the same parameters. In Fig. 5, we plot the results for the start and end flux biases of Fig. 3 using the fitted parameters of $I_c = 0.84$ μA, $L = 757$ pH, $C = 743$ fF from the second approach, which are close to the designed values described above. At $\Phi_e/\Phi_0 = 0.51$, the energy level numbers are 20 and 26 in the left and right potential wells while at $\Phi_e/\Phi_0 = 0.565$, they are 6 and 45. These results indicate that the energy spectrum in Fig. 3 covers almost the entire measurable flux bias range. At the start flux bias, the qubit level spacing in the left potential well becomes discriminable from the corresponding spacing in the right potential well. At the end flux bias, the qubit state in the left potential well still has a negligible macroscopic tunneling rate.

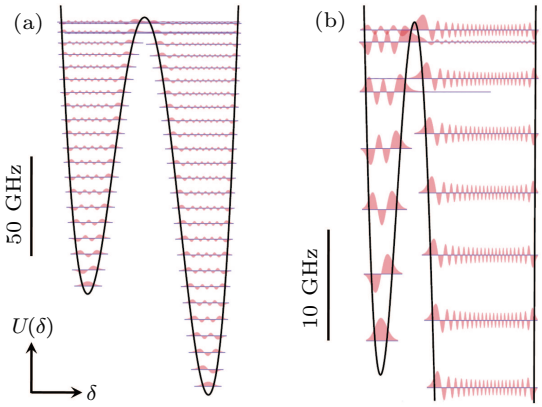


Fig. 5. (color online) Potential wells (black lines), energy levels (thin blue lines), and wave functions (red areas) of the phase qubit at two flux biases of (a) $\Phi_e = 0.510\Phi_0$ and (b) $\Phi_e = 0.565\Phi_0$, which correspond to the start and end biases in Fig. 3. Note that the two lowest levels in the left potential well are considered as the qubit levels in each case of the flux biases.

There are several possible places where incoherent or weakly-coupled coherent TLS may reside to cause the qubit decoherence: The bulk dielectric substrate, the oxidized surface layer of the substrate, the metal-dielectric interface, or a thin dielectric layer formed on the metal and/or dielectric surfaces when exposed to air during the fabrication process.[27–31] To improve the qubit coherence, therefore, sapphire or unoxidized Si substrates with careful surface treatment[27–31] may be used to replace the present oxidized Si substrates. To do so several additional points in the above-described fabrication process should be considered. In the case of insulating sapphire substrates, special care needs to be taken with the e-beam lithographic patterning due to the charge store-up during resist exposure. For the unoxidized Si substrates, dry etching of the Nb and Si layers in SF_6 should be precisely controlled duo to the fast etching rate of the Si substrate. In addition, it will be helpful to use TiN instead of Nb for the outer circuits shown in Fig. 2(a). The TiN film is known to be much more resistant to oxidation when exposed air, as compared to the Nb films used in the present experiment, and can also be dry etched conveniently in SF_6. Further improvements for the qubit performance need to be made along these directions.

4. Summary

We have developed a fabrication process for superconducting phase qubits in which Josephson junctions for both the qubit and SQUID detector were prepared by the technique of

shadow evaporation with suspended bridge. Using this technique, junctions with areas as small as 0.05 μm^2 were fabricated for the qubit so that the number of quantum TLS causing qubit decoherence could be greatly reduced. In contrast to the previous reports, the measurements of the energy spectrum and vacuum Rabi process showed no coherent TLS present in the entire flux bias range of the phase qubit, which was confirmed by the numerical simulation of the qubit system. However, the measured results also indicated the presence of incoherent TLS coupled to the qubit and showed the relaxation time T_1 and dephasing time T_φ on the order of 100 ns and 50 ns, respectively, which are a few factors shorter compared to the best reported results of the Al phase qubits.[8,9] We discussed several possible origins for the qubit decoherence from the surface oxide layer of the Si substrate and the surface or interface dielectric layers of the metal and Si films formed when exposed to air during the fabrication process. These can be avoided by using substrates such as sapphire or unoxidized Si and using superconducting films such as TiN instead of Nb for the outer circuits. Further improvements of the phase qubit performance are therefore expected in the future studies taking these considerations into account.

Acknowledgments

We thank Siyuan Han and H Wang for helpful discussions. We are grateful to the Laboratory of Microfabrication at the Institute of Physics for technical help.

References

[1] Clarke J and Wilhelm F K 2008 *Nature* **453** 1031
[2] Devoret M H and Schoelkopf R J 2013 *Science* **339** 1169
[3] You J Q and Nori F 2011 *Nature* **474** 589
[4] Georgescu I M, Ashhab S and Nori F 2014 *Rev. Mod. Phys.* **86** 153
[5] Simmonds R W, Lang K M, Hite D A, Nam S, Pappas D P and Martinis J M 2004 *Phys. Rev. Lett.* **93** 077003
[6] Martinis J M, Cooper K B, McDermott R, Steffen M, Ansmann M, Osborn K D, Cicak K, Oh S, Pappas D P, Simmonds RW and Yu C C 2005 *Phys. Rev. Lett.* **95** 210503
[7] Neeley M, Ansmann M, Bialczak R C, Hofheinz M, Katz N, Lucero E, O'Connell A, Wang H, Cleland A N and Martinis J 2008 *Phys. Rev. B* **77** 180508
[8] Martinis J M 2009 *Quantum Inf. Process.* **8** 81
[9] Weides M, Bialczak R C, Lenander M, Lucero E, Mariantoni M, Neeley M, O'Connell A D, Sank D, Wang H, Wenner J, Yamamoto T, Yin Y, Cleland A N and Martinis J 2011 *Supercond. Sci. Technol.* **24** 055005
[10] Lecocq F, Pop I M, Peng Z H, Matei I, Crozes T, Fournier T, Naud C, Guichard W and Buisson O 2011 *Nanotechnology* **22** 315302
[11] Sank D, Barends R, Bialczak R C, Chen Y, Kelly J, Lenander M, Lucero E, Mariantoni M, Megrant A, Neeley M, O'Malley P J J, Vainsencher A, Wang H, Wenner J, White T C, Yamamoto T, Yin Y, Cleland A N and Martinis J M 2012 *Phys. Rev. Lett.* **109** 067001
[12] Whittaker J D, da Silva F C S, Allman M S, Lecocq F, Cicak K, Sirois A J, Teufel J D, Aumentado J and Simmonds R W 2014 *Phys. Rev. B* **90** 024513
[13] Martinis J M and Megrant A 2014 arXiv: 1410.5793
[14] Tan X S, Yu H F, Yu Y and Han S 2015 *Appl. Phys. Lett.* **107** 102601
[15] Lecocq F, Teufel J D, Aumentado J and Simmonds R W 2015 *Nat. Phys.* **11** 635
[16] Lisenfeld Jürgen, Grabovskij Grigorij J, Müller Clemens, Cole Jared H, Weiss Georg and Ustinov Alexey V 2015 *Nat. Commun.* **6** 6182
[17] Lisenfeld Jürgen, Bilmes Alexander, Matityahu Shlomi, Zanker Sebastian, Marthaler Michael, Schechter Moshe, Schön Gerd, Shnirman Alexander, Weiss Georg and Ustinov Alexey V 2016 *Sci. Rep.* **6** 23786
[18] Nakamura Y, Pashkin Y A and Tsai J S 1999 *Nature* **398** 6730
[19] Vion D, Aassime A, Cottet A, Joyez P, Pothier H, Urbina C, Esteve D, and Devoret M H 2002 *Science* **396** 886
[20] Orlando T P, Mooij J E, Tian L, van der Wal C H, Levitov L S, Lloyd S and Mazo J J 1999 *Phys. Rev. B* **60** 15398
[21] Chiorescu I, Nakamura Y, Harmans C J P M and Mooij J E 2003 *Science* **299** 1869
[22] Koch J, Yu T M, Gambetta J, Houck A A, Schuster D I, Majer J, Blais A, Devoret M H, Girvin S M and Schoelkopf R J 2007 *Phys. Rev. A* **76** 042319
[23] Barends R, Kelly J, Megrant A, Sank D, Jeffrey E, Chen Y, Yin Y, Chiaro B, Mutus J, Neill C, O'Malley P, Roushan P, Wenner J, White T C, Cleland A N and Martinis J M 2013 *Phys. Rev. Lett.* **111** 080502
[24] Tian Ye, Yu H F, Deng H, Xue G M, Liu D T, Ren Y F, Chen G H, Zheng D N, Jing X N, Lu Li, Zhao S P and Han Siyuan 2012 *Rev. Sci. Instrum.* **83** 033907
[25] Mao Bo 2010 "Coherent Manipulation of Multi-Partite Quantum States in a Qubit-TLS System via Landau-Zener Transition", Ph. D thesis, University of Kansas
[26] Dutta P, Adhikari S and Bhattacharyya S P 1993 *Chem. Phys. Lett.* **212** 677
[27] Wang H, Hofheinz M, Wenner J, Ansmann M, Bialczak R C, Lenander M, Lucero Erik, Neeley M, O'Connell A D, Sank D, Weides M, Cleland A N and Martinisa J M 2009 *Appl. Phys. Lett.* **95** 233508
[28] Wenner J, Barends R, Bialczak R C, Chen Yu, Kelly J, Lucero Erik, Matteo Mariantoni, Megrant A, O'Malley P J J, Sank D, Vainsencher A, Wang H, White T C, Yin Y, Zhao J, Cleland A N and Martinis J M 2011 *Appl. Phys. Lett.* **99** 113513
[29] Sage Jeremy M, Bolkhovsky Vladimir, Oliver William D, Turek Benjamin and Welander Paul B 2011 *J. Appl. Phys.* **109** 063915
[30] Megrant A, Neill C, Barends R, Chiaro B, Chen Yu, Feigl L, Kelly J, Lucero Erik, Mariantoni Matteo, O'Malley P J J, Sank D, Vainsencher A, Wenner J, White T C, Yin Y, Zhao J, Palmstrfm C J, Martinis John M and Cleland A N 2012 *Appl. Phys. Lett.* **100** 113510
[31] Bruno A, de Lange G, Asaad S, van der Enden K L, Langford N K and DiCarlo L 2015 *Appl. Phys. Lett.* **106** 182601